The Astrophysical Journal, 955:86 (10pp), 2023 October 1 https://doi.org/10.3847/1538-4357/acf1fb

QPOs in Compact Sources as a Nonlinear Hydrodynamical Resonance: Determining Spin of Compact Objects

Arghya Ranjan Das and Banibrata Mukhopadhyay
Department of Physics, Indian Institute of Science, Bangalore 560012, India; arghyadas@iisc.ac.in, bm@iisc.ac.in
Received 2023 June 3; revised 2023 August 16; accepted 2023 August 17; published 2023 September 21

Abstract

The origin of wide varieties of quasiperiodic oscillations (QPOs) observed in compact sources is still not well established. Its frequencies range from millihertz to kilohertz spanning all compact objects. Are different QPOs, with different frequencies, originating from different physics? We propose that the emergence of QPOs is the result of nonlinear resonance of fundamental modes present in accretion disks forced by external modes including that of the spin of the underlying compact object. Depending on the properties of accreting flow, e.g., its velocity and gradient, resonances (and any mode-locking) take place at different frequencies, exhibiting low- to high-frequency QPOs. We explicitly demonstrate the origin of higher-frequency QPOs for black holes and neutron stars by a unified model and outline how the same physics could be responsible for producing lower-frequency QPOs. The model also predicts the spin of black holes, and constrains the radius of neutron stars and the mass of both.

Unified Astronomy Thesaurus concepts: Black hole physics (159); Neutron stars (1108); Accretion (14); Gravitation (661); Hydrodynamics (1963); Stellar oscillations (1617)

1. Introduction

Since its first discovery in the 1980s (Motch et al. 1983; van der Klis et al. 1985), there have been numerous discoveries of quasiperiodic oscillations (QPOs) with their varieties of properties in the black hole and neutron star sources, even sometimes in white dwarfs (e.g., Mauche 2002; Titarchuk & Wood 2002; Woudt & Warner 2002). While for neutron stars, QPOs are mostly observed on the order of kilohertz frequencies, for black holes they vary from the fraction of hertz to the fraction of kilohertz; the latter is called the high-frequency (HF) QPO. While HF QPOs are observed mainly in the high-soft (HS) state of a black hole system (Belloni et al. 2012), the low-frequency QPOs are mostly observed in harder states (Belloni et al. 2012; Motta et al. 2012; Franchini et al. 2016). Moreover, often the source exhibits jets along with low-frequency QPOs in a hard state, e.g., in a canonical low-hard (LH) state.

Often the kilohertz/HF QPOs appear with a pair. It had been argued and apparently observed that the separation between the kilohertz QPO frequencies in a pair is similar in order of magnitude to the half of the spin frequency or the spin frequency itself of the fast or slowly rotating neutron stars, respectively (van der Klis 2000; Kluźniak et al. 2004). This argues for a relation between kilohertz QPOs and the spin of neutron stars. On the other hand, the HF QPOs in a pair for black holes were argued to be in a 3:2 ratio (Rezzolla et al. 2003; Remillard & McClintock 2006; Török et al. 2015); but also see Homan et al. 2003, whose observational analysis argued against it, even though some authors argued QPOs from the neutron star, Sco X-1, appear in this ratio (Abramowicz et al. 2003a; Rebusco 2008). Alternative viewpoints have been put forth suggesting against the fixed 3:2 ratio, and instead suggesting a multipeaked distribution of QPO frequencies for Sco X-1 and other sources, namely, 4U 160852, 4U 1636-53, 4U 1728-34, and 4U 1820-30, with the ratio of high- to low-frequency QPOs being 3/2, 4/3, 5/4, 7/5, and 9/7 spanning around sources; not all ratios appear in all sources though (Belloni et al. 2005, 2007).

Now the question arises, could all of the QPOs, particularly the kilohertz/HF ones, originate from the same mechanism? Generally, the QPOs are expected to be processed in the matter inflowing toward compact objects, i.e., in the accretion disk therein, probably in its inner region where the effect of gravity is stronger. Therefore, it is expected to originate from the same/similar mechanism, broadly independent of the nature of the compact object, which is primarily controlled by gravity. Therefore, we target explaining the origin of (kHz/HF) QPOs by a unified mechanism in an accretion flow.

Often kilohertz/HF QPOs are argued to be involved with parametric resonance phenomena and related mode-locking (Stella & Vietri 1998; Stella et al. 1999; Lamb & Miller 2001; Cadez et al. 2008; Kostic et al. 2009; Germana et al. 2009; Kluzniak & Abramowicz 2002; Abramowicz et al. 2003b; Rebusco 2004; Nowak et al. 1997; Torok et al. 2010, 2011; Kotrlová et al. 2020). Mukhopadhyay (2009) initiated modeling, both kilohertz QPOs of neutron stars and HF QPOs of black holes in a unified scheme. The author argued, based on a very schematic model, the kilohertz/HF QPOs to be the result of higher-order nonlinear processes in accretion disks. Based on this QPO model, the spin of black holes and neutron stars (if unknown) was also estimated. Since QPO carries the information of spacetime around the compact object, it can also be used to test any modification to gravity, such as asymptotically flat modified $f(R)$-gravity (Kalita & Mukhopadhyay 2019; Das & Mukhopadhyay 2022) in a strong gravity regime.

Arguably, the HF QPOs are the most reliable source of spin measurement once the correct model is known (Remillard & McClintock 2006). There are many avenues in which a black hole's spin measurement can be done such as polarimetry (Connors et al. 1980; Lightman & Shapiro 1975), continuum fitting (Zhang et al. 1997; Dovčiak et al. 2004; Davis et al. 2005;

Li et al. 2005; Kulkarni et al. 2011), the Fe K line (Reynolds & Nowak 2003; Reynolds & Fabian 2008), and HFQPOs (e.g., Mukhopadhyay 2009). Arguably the best current method, continuum fitting, has the drawback that it requires precise estimations of parameters such as black hole mass (M), disk inclination (i), and distance. On the other hand, assuming that we have a well-tested QPO model, spin estimation would require only an estimation of M. In fact, our current model constrains the already existing mass range further to a more precise estimation from the observed QPO frequencies.

Earlier it was shown that QPOs may arise due to nonlinear resonance phenomena in accretion disks placed in strong gravity (Kluźniak et al. 2004; Pétri 2005; Blaes et al. 2007). The hydrodynamic/magnetohydrodynamic equations that govern the accretion dynamics and disk structure are nonlinear; hence, a nonlinear response is expected. In the present work, we propose a modification to the epicyclic frequencies due to motion of fluid (instead of test particle) around the compact object. We consider these modified frequencies as fundamental modes to model QPO frequencies based on nonlinear dynamics and resonance following the approach of Mukhopadhyay (2009). The model successfully describes the observational trends in QPOs and is able to reproduce the observed frequencies. In the process of reproducing observed results, the model estimates the mass (M) and spin parameter (a) of the black holes and radius of neutron stars, and also an estimate of spin frequency of neutron star (if unknown) is made.

The plan of the paper is as follows. In the next section we derive the modified epicyclic frequencies for fluids around a compact object. Section 3 devotes outlining the basic properties of nonlinear resonance and how does it govern QPOs in the accretion disk. Subsequently, we outline the basic characteristics of black holes and neutron stars and their basic parameters required for our model in Section 4. Sections 5 and 6 explore our model to explain observed QPOs for neutron stars and black holes, respectively. Before concluding, we outline in Section 7 that our model could explain other QPO frequencies as well. Finally, we end with a summary and conclusions in Section 8.

2. Modified Epicyclic Frequency for Fluid

We consider a small annulus region of an accretion disk. This small region is assumed to be incompressible, and the momentum balance is given by

$$\frac{\partial \boldsymbol{u}}{\partial t} + (\boldsymbol{u}\cdot\nabla)\boldsymbol{u} + \nabla\left(\frac{P}{\rho_0}\right) = \boldsymbol{F}, \tag{1}$$

where $\boldsymbol{u}$, P and ρ_0 are the velocity, pressure, and density of the fluid, respectively, and $\boldsymbol{F}$ is the external force per unit mass including the contribution due to gravity.

Now consider a fluid packet to be moving at a radius $\boldsymbol{r}$. Due to several possible sources of disturbances in general, we consider a small orbital perturbation of the fluid packet as

$$\boldsymbol{r} \rightarrow \boldsymbol{r} + \delta\boldsymbol{r}. \tag{2}$$

Assuming locally polytropic equation of state, from Equations (1) and (2), the linearly perturbed equation takes the form of

$$\frac{\partial \delta\boldsymbol{u}}{\partial t} + (\delta\boldsymbol{u}\cdot\nabla)\boldsymbol{u} + (\boldsymbol{u}\cdot\nabla)\delta\boldsymbol{u} = \delta\boldsymbol{F}, \tag{3}$$

where the quantities under δ imply the perturbation of the original variables. Combining the first and third terms from Equation (3), we have

$$\frac{d\delta\boldsymbol{u}}{dt} + (\delta\boldsymbol{u}\cdot\nabla)\boldsymbol{u} = \delta\boldsymbol{F}. \tag{4}$$

This equation effectively describes a forced damped oscillator. We further confine the equatorial accretion disk around compact objects assuming axisymmetry. Hence, the second term in Equation (4) in a cylindrical coordinate system can be broken down to its components as

$$(\delta\boldsymbol{u}\cdot\nabla)\boldsymbol{u} = \left[\delta u_r\left(\frac{\partial u_r}{\partial r}\right) - \left(\frac{u_\phi}{r}\right)\delta u_\phi\right]\hat{r} + \delta u_r\left(\frac{\partial u_\phi}{\partial r}\right)\hat{\phi}. \tag{5}$$

Now we should note that $u_\phi = r\dot{\phi} \equiv r\Omega_\phi$, and thus due to separation of orbits, we can write

$$\begin{aligned}\frac{d\delta u_\phi}{dt} &= \frac{d}{dt}(r\delta\dot{\phi} + \Omega_\phi\delta r)\\ &= r\delta\ddot{\phi} + \Omega_\phi\delta\dot{r},\end{aligned} \tag{6}$$

assuming effectively circular orbit when $u_r = \dot{\Omega}_\phi \sim 0$. Thus from Equations (4), (5), and (6), the components of the perturbed momentum balanced equation can be written as

$$\delta\ddot{r} + \gamma\delta\dot{r} - \Omega_\phi(r\delta\dot{\phi} - \Omega_\phi\delta r) = (\delta\boldsymbol{F})_r, \tag{7}$$

$$\delta\ddot{z} = (\delta\boldsymbol{F})_z, \tag{8}$$

$$r\delta\ddot{\phi} + \Omega_\phi\delta\dot{r} + \xi\delta\dot{r} = (\delta\boldsymbol{F})_\phi, \tag{9}$$

where $\xi = r\Omega_{\phi,r}$ and $\gamma = \partial u_r/\partial r$.

Now we consider the change (or the perturbation) in the force due to two reasons, one is due to the orbital perturbation and the other is due to the presence of some forcing in the system. Thus, the combined perturbed force will take the form of

$$\delta\boldsymbol{F} = \boldsymbol{F}_{\rm forced} + \delta\boldsymbol{F}_{\rm orbit}, \tag{10}$$

where the change in the orbital force in the axisymmetric equatorial system becomes

$$\delta\boldsymbol{F}_{\rm orbit} = -(\Omega_r^2\delta r)\hat{r} - (\Omega_z^2\delta z)\hat{z}. \tag{11}$$

The term Ω_j can be written as $\Omega_j = 2\pi\nu_j$ such that the frequencies ν_r and ν_z are the epicyclic frequencies, and ν_ϕ is the orbital frequency of a test particle moving in the equatorial circular orbit around the compact object. In the Kerr metric, these frequencies are given as

$$\nu_\phi = \frac{1}{2\pi}\frac{1}{r^{3/2} + a}\frac{c^3}{GM}, \tag{12}$$

$$\nu_r = \frac{\nu_\phi}{r}\sqrt{\Delta - 4(\sqrt{r} - a)^2}, \tag{13}$$

$$\nu_z = \frac{\nu_\phi}{r}\sqrt{r^2 - 4a\sqrt{r} + 3a^2}, \tag{14}$$

where $\Delta = r^2 - 2r + a^2$, M is the mass of the central compact object, G is Newton's gravitational constant, and c is the speed of light. For simplicity, we take the force to be varying with

some frequency ω, of the form,

$$\boldsymbol{F}_{\rm forced} = (F_{0r}\hat{r} + F_{0z}\hat{z} + F_{0\phi}\hat{\phi})\cos\omega t. \quad (15)$$

Hence, the following equations of perturbation can be written from Equations (7), (8), (9), (11), and (15) as

$$\delta\ddot{r} + \gamma\delta\dot{r} - \Omega_\phi(r\dot{\delta\phi} - \Omega_\phi\delta r) = -\Omega_r^2\delta r + F_{0r}\cos\omega t, \quad (16)$$

$$\delta\ddot{z} = -\Omega_z^2\delta z + F_{0z}\cos\omega t, \quad (17)$$

$$r\ddot{\delta\phi} + \Omega_\phi\delta\dot{r} + \xi\delta\dot{r} = F_{0\phi}\cos\omega t. \quad (18)$$

The above equations are similar to the components of the equation describing the forced damped harmonic oscillator. As a solution technique, we choose the force $F_{0j}\cos\omega t$ as $F_{0j}e^{i\omega t}$ (actually the real part of it), where $j \in \{r, z, \phi\}$, and we make the ansatz that all of the perturbations will have the form

$$\delta r = \mathcal{R}(\omega)e^{i\omega t}, \quad (19)$$

$$\delta z = \mathcal{Z}(\omega)e^{i\omega t}, \quad (20)$$

$$\delta\phi = \Phi(\omega)e^{i\omega t}. \quad (21)$$

Putting Equations (19), (20), and (21) in Equations (16), (17), and (18), we obtain three equations for $\mathcal{R}(\omega)$, $\mathcal{Z}(\omega)$ and $\Phi(\omega)$, which can be solved. As a first case, for simplicity, we assume $F_{0r} = F_{0z} = F_{0\phi} = F_0$. Having this, the solution for the amplitudes can be found to be of the form

$$\mathcal{R}(\omega) = \frac{F_0(\omega - i\Omega_\phi)}{\omega[\Omega_\phi(\xi + 2\Omega_\phi) + i\omega(\gamma + i\omega) + \Omega_r^2]} \quad (22)$$

$$\mathcal{Z}(\omega) = -\frac{F_0}{\omega^2 - \Omega_z^2} \quad (23)$$

$$\Phi(\omega) = -\frac{F_0[-i\omega(\xi - \gamma - i\omega) + \Omega_r^2 - i\omega\Omega_\phi + \Omega_\phi^2]}{\omega^2 r[\Omega_\phi(\xi + 2\Omega_\phi) + i\omega(\gamma + i\omega) + \Omega_r^2]}. \quad (24)$$

The absolute values of the amplitudes (i.e., those up to a phase factor), are given by

$$|\mathcal{R}(\omega)| = \frac{|F_0|\sqrt{\omega^2 + \Omega_\phi^2}}{\omega\sqrt{\gamma^2\omega^2 + [\Omega_\phi(\xi + 2\Omega_\phi) + \Omega_r^2 - \omega^2]^2}}, \quad (25)$$

$$|\mathcal{Z}(\omega)| = \frac{|F_0|}{\omega^2 - \Omega_z^2}, \quad (26)$$

$$|\Phi(\omega)| = \frac{|F_0|\sqrt{\omega^2(\xi - \gamma + \Omega_\phi)^2 + (\Omega_r^2 - \omega^2 + \Omega_\phi^2)^2}}{\omega^2 r\sqrt{\gamma^2\omega^2 + [\Omega_\phi(\xi + 2\Omega_\phi) + \Omega_r^2 - \omega^2]^2}}. \quad (27)$$

Therefore, the perturbation δz is maximized when we have

$$\omega = \Omega_z, \quad (28)$$

and δr and $\delta\phi$ are at maximum when

$$f(\omega) = \gamma^2\omega^2 + [\Omega_\phi(\xi + 2\Omega_\phi) + \Omega_r^2 - \omega^2]^2 \quad (29)$$

is at minimum. It can be easily found that $f(\omega)$ is minimized for $\gamma = 0$ (for a circular orbit) when

$$\omega = \sqrt{r\Omega_\phi + \Omega_r^2 + 2\Omega_\phi^2}. \quad (30)$$

Thus, from Equations (28) and (30), we obtain the modified epicyclic frequencies for fluids moving in an accretion disk in the equatorial circular orbit, hence in a Keplerian accretion disk, denoted as ν_1 and ν_2, given by

$$\nu_1 = \sqrt{\nu_r^2 + 2\nu_\phi^2 + r\nu_{\phi,r}\nu_\phi}, \quad (31)$$

$$\nu_2 = \nu_z. \quad (32)$$

This modification can be summarized to be that the vertical epicyclic frequency remains unchanged as given by that of a test particle, as in ν_2. However, there is a combination of the radial epicyclic frequency and the orbital frequency, as defined for a test particle, leading to a new epicyclic frequency for fluid as ν_1.

3. Nonlinear Resonance and QPO

In the nonlinear regime, a perturbation at the stellar spin frequency ν_s can weakly excite a disk motion at the same frequency. This is expected as a rotating central object may influence the disk fluid. If a mode frequency is already present along with the perturbing frequency, another mode can be excited at a combination of the frequencies (Landau & Lifshitz 1976; Abramowicz et al. 2003b). In addition, if the frequency difference of two said modes excited in a system is close to $p\nu_s$, a resonance may occur such that the system is responsive to this frequency difference only (where p is a number such as $n/2$, and n is an integer, for instance, 1 or 2 in the present model). This resonance leads to mode-locking. Indeed some neutron star systems show that the frequency difference between twin kilohertz QPOs remains close to the stellar spin frequency or the half the spin frequency, even though the QPO frequencies vary over time (van der Klis 2000).

The underlying concept is that when a compact object rotates, it creates a new mode in the surrounding region corresponding to the spin frequency ν_s, which couples to those corresponding to ν_1 and ν_2, already existing in the disk. This coupling will lead to the emergence of new modes with frequencies $\nu_{1,2} \pm p\nu_s$. Now at a certain radius if the difference of ν_1 and ν_2 is close to zero and, additionally, if $\nu_s/2$ (for nonlinear regime) or ν_s (for linear regime) is close to the frequency difference of any two newly excited modes, a resonance may occur. This resonance will cause the frequency difference of two excited modes to lock at $\nu_s/2$ or ν_s.

Now for instance a system with l degrees of freedom has l linear natural frequencies and modes denoted by $\nu_1, \cdots, \nu_l$ with all being real and nonzero. Then if the frequencies are commensurable or nearly commensurable, the system exhibits a strong frequency coupling, giving rise to internal resonance (Nayfeh & Mook 1979). In addition, if there exists a harmonic external excitation frequency ν_s, then the frequencies might have a commensurable relationship exhibiting the resonance as

$$p\nu_s = \Sigma_{i=1}^{l} b_i\nu_i, \quad (33)$$

where p and b_i are integers such that

$$p + \Sigma_{i=1}^{n}|b_i| = k + 1, \quad (34)$$

where k is the order of nonlinearity.

As described in Section 2, we know that the fundamental frequencies of the accretion system will be the modified epicyclic frequencies for the fluid system as given by Equations (31) and (32). Therefore, similar to Mukhopadhyay (2009), we rewrite Equation (33) for an accretion disk with the

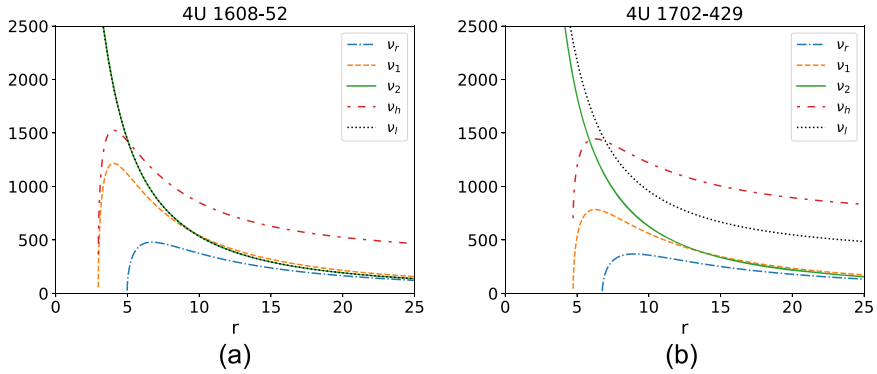

Figure 1. Variation of different frequencies (in hertz) as a function of distance from the central object in units of gravitational radius in the accretion disk, where (a) 4U 1608-52 is a fast rotator with the resonance radius $r = 9.49GM/c^2$, and (b) 4U 1702-429 is a slow rotator with the resonance radius $r = 13.8GM/c^2$. The values of m are chosen to be 0 and 1, respectively, so that they lead to the reasonable radii, as given in Table 1.

2 degrees of freedom with corresponding frequencies ν_1 and ν_2 as

$$(n - m + 1)\nu_s = b_1\nu_1 + b_2\nu_2. \tag{35}$$

3.1. Nonlinear Regime

Here we take $b_1 = -b_2 = 2$, which leads to

$$\frac{\nu_s}{2}(n - m + 1) = \nu_1 - \nu_2, \tag{36}$$

with m and n being integers. In the disk around a neutron star, at an appropriate radius where $\nu_1 - \nu_2 \approx 0$, the resonance is supposed to take place, which from Equation (36) gives $n = m - 1$. Now we propose the higher and lower QPO frequencies of a pair to be, respectively,

$$\nu_h = \nu_1 + \frac{m+1}{2}\nu_s, \quad \nu_l = \nu_2 + \frac{m}{2}\nu_s. \tag{37}$$

After rearranging the terms of Equation (36), we obtain the relation as

$$\left(\nu_1 + \frac{m+1}{2}\nu_s\right) - \left(\nu_2 + \frac{m}{2}\nu_s\right) = \frac{\nu_s}{2}. \tag{38}$$

From our proposed QPO frequencies and resonance condition, we see that the condition for $\Delta\nu$ is satisfied as

$$\Delta\nu = \nu_h - \nu_l \approx \frac{\nu_s}{2}. \tag{39}$$

Figure 1 (left panel) shows the formation of the above resonance and QPOs at around $r = 9.49GM/c^2$. At this radius, $\nu_1 = \nu_2$ and $\Delta\nu \sim \nu_s/2$. The neutron star mentioned there is reported in the following section.

The observed phenomenon of the frequency difference between twin kilohertz QPOs remaining close to the half of the stellar spin frequency (or the stellar spin frequency itself, as explained below) in many neutron star systems, even if the QPO frequencies vary over time, can be explained by the above model. Even though the excitation order m changes, the difference in the high and low frequencies remains the same.

3.2. Linear Regime

However, for a black hole due to the absence of a magnetosphere and a weakly magnetized neutron star, the coupling between modes may not be nonlinear, and resonance locking may occur in the linear regime when the condition that $\nu_h - \nu_l$ is approximately equal to ν_s is met. For this condition, we just have to take the first-order excitation in Equation (35) and put $b_1 = -b_2 = 1$, and following the same strategy, as in nonlinear regime, the QPO frequencies take the form

$$\nu_h = \nu_1 + (m + 1)\nu_s, \tag{40}$$

$$\nu_l = \nu_2 + m\nu_s. \tag{41}$$

It is evident from Equations (40) and (41) that the condition for resonance $\Delta\nu \approx \nu_s$ is satisfied. Figure 1 (right panel) shows that at $r = 13.8GM/c^2$ the linear resonance forms with $\nu_1 = \nu_2$ and $\Delta\nu \sim \nu_s$. The mentioned neutron star therein is reported in the following section.

4. Basic Characteristics of Black Holes and Neutron Stars

As mentioned above, there is a subtle difference in the resonance conditions for the formation of QPOs around black holes and neutron stars. This may be attributed to the disparities in their environment. In the case of a magnetized neutron star particularly, the oscillations of the disk are directly influenced by the rotating magnetosphere, which imprints the spin frequency of the star leading to a resonance. However, for a black hole, the energy and angular momentum may be transferred to the surrounding region through the magnetic field lines, which however may not be as strong as for neutron stars, particularly for soft states (Blandford & Znajek 1977). This is expected to lead to a strong resonance, to be driven by the disturbances at the spin frequency of the black hole, although the exact mechanism is yet to be determined. Additionally, it should be noted that while the presence of a hard surface of a neutron star leads to a strict definition of ν_s corresponding to its boundary layer related to the spin parameter a, there is no such definition for a black hole. Nevertheless, here we assume that the spin of the black is experienced by the accreting fluid through the frame-dragging frequency.

The spin frequency of a neutron star can be asserted from observed data. However, in computing the QPO frequencies from our model, we also need to determine the dimensionless spin parameter a. Assuming the neutron star to be almost spherically symmetric with the equatorial radius R, spin frequency ν_s, mass M, the radius of gyration R_G, the moment of inertia and the spin parameter, respectively, can be defined

as

$$I = MR_G^2, \quad a = \frac{I\Omega_s}{\frac{GM^2}{c}}, \tag{42}$$

where $\Omega_s = 2\pi\nu_s$. However, for a black hole, mass M and a are the most natural parameters that we supply as inputs. The corresponding frame-dragging angular frequency on the space-time around the black hole is then given by

$$\Omega_{\rm BH} = -\frac{g_{\phi t}}{g_{\phi\phi}} = \frac{2a}{r^3 + ra^2 + 2a^2}, \tag{43}$$

and, thus, for a black hole, we define the spin frequency as

$$\nu_{\rm BH} = \nu_s = \frac{\Omega_{\rm BH}}{2\pi}\frac{c^3}{GM}, \tag{44}$$

which is actually the imprint of spin frequency at a given radius away from the black hole. Therefore, by supplying the spin parameter a, mass M, and the radius r, the effective spin frequency can be determined.

5. Properties of Neutron Star QPO

It has been observed that QPO frequencies tend to vary over time, with the frequency difference between them in a pair decreasing slightly as the lower QPO frequency increases. As mentioned above, for fast rotators, the frequency difference is approximately half of the spin frequency, whereas for slow rotators, it is of the same order as the spin frequency. Our model successfully explains these observed properties as demonstrated below. To obtain our results, we explore a suitable range of mass of the neutron star M and the spin parameter a. For ν_l and ν_h, we use the Kerr metric only, as given by Equations (12), (13), (14), (31), and (32). However, strictly speaking, the Kerr metric is for black holes. Nevertheless, for the present purpose, it does not matter practically as we are interested outside of a neutron star and also not to close to it. Now, using the grid search algorithm, we find the parameters that fit the observational data the best. Basically, we try to find out the parameters that make reduced $\chi^2 = \sum_i (O_i - C_i)^2/\sigma_i^2 D$ close to unity; here, O_i and C_i are observed and our model computed values corresponding to the $i^{\rm th}$ observation, respectively, with σ_i as the variance of measurement error and D being the degrees of freedom (i.e., the number of observed data points minus the number of fitted parameters). Our aim should be to align χ^2 as close to unity as possible. A suitable function to gauge the closeness of $\chi^2 \to 1$ would be $f(\chi^2) = |1 - \chi^2|$. This function reaches its minimum value of zero when $\chi^2 \to 1$, thus implying a good fit. Therefore, we plan to find the parameters that minimize f (ideally $\to 0$), thereby ensuring that χ^2 is as near to 1 as possible, indicative of an optimal fit.

5.1. Fast Rotators

We analyze the QPOs of some of the fast rotating neutron stars whose spin frequencies are known: KS 1731-260 (Smith et al. 1997), 4U 1636-53 (Jonker et al. 2002), and 4U 1608-52 (Méndez et al. 1998). We vary the mass M and the spin parameter a in appropriate and/or admissible ranges and find their suitable values giving the best fit for the observed QPOs based on our model.

We know that for a solid sphere we have $R_G^2 = 2R^2/5$ and for a hollow sphere $R_G^2 = 2R^2/3$. It is known that neutron stars are not perfect solid bodies and are expected to be deformed from a perfect spherical to an ellipsoidal shape at very fast rotation rates. Hence, in our calculation, we consider a range $0.35 \leqslant (R_G/R)^2 \leqslant 0.5$ for most cases, as suggested in previous studies (Bejger & Haensel 2002; Cook et al. 1994; Mukhopadhyay 2009). Hence, from Equation (42), we have the radius of the neutron star in the range

$$\frac{R_G}{\sqrt{0.35}} \leqslant R \leqslant \frac{R_G}{\sqrt{0.5}}, \tag{45}$$

where $R_G = \sqrt{GMa/2\pi\nu_s c}$. Table 1 shows the estimated parameters that best fit the observed QPOs based on our model.

KS 1731-260, to date, has exhibited only one pair of QPO frequencies, established by our model and is depicted in Figure 2. However, due to its single data point, many parameters can reproduce the observed QPO frequencies within the error bound. Therefore, we only consider the nonlinear regime for $m = -1$, 0, and 1. We also find that considering other values of m or linear regime gives a radius $R > 12.5$ km, which is strongly restricted by Özel et al. (2012). Using our model, we obtain $M = 1.51M_\odot$ with a radius between 10.08 km and 12.04 km; $M = 1.2M_\odot$ with a radius in 10.32 km and 12.33 km; and $M = 1.07M_\odot$ with a radius in 10.99 km and 13.14 km, for $m = -1$, 0, and 1, respectively. However, if we allow a lower mass and radius, e.g., like a strange star, our model also produces this result (see, e.g., Mukhopadhyay et al. 2003), shown for one such a case in Table 2.

For 4U 1636-53 and 4U 1608-52, however, several twin peak QPOs have been observed varying with time. Although the high and low QPO frequencies vary, their difference remains almost constant with a slightly decreasing trend with the increasing lower QPO frequency. This trend has been successfully reproduced, and the observed QPOs have been fitted very well by our model.

For 4U 1636-53, from the data it is evident that the source is in a nonlinear regime like other fast rotators. But $\Delta\nu$, though remains constant for lower ν_l, decreases a little more rapidly with increasing ν_l, compared to other cases. Hence, this gives a rather poor fitting if we consider activation of only one mode m, as shown in Figure 2. However, it could be possible that two harmonics (or modes), say m_1 and m_2, are activated at various times of observations, and not considering both of the modes appropriately in the analysis results in a poor fit. To address this issue, we vary the mass M and spin parameter a for two values of m: m_1 and m_2. This gives two sets of curves for a given M and a in the nonlinear regime, yielding two sets of parameters (with two modes or m values), as shown in Figure 2. One set results in a mass of $M = 1.5M_\odot$, corresponding to a neutron star radius range of $14.52\,{\rm km} \leqslant R \leqslant 17.35$ km, a bit large, for $m = -2, -1$. The other set results in a mass of $M = 1.65M_\odot$, corresponding to a neutron star radius range of $15.61\,{\rm km} \leqslant R \leqslant 18.66$ km, even larger, for $m = -2$, 0. However, for $m = -1$, 1, with a slightly lower mass $M = 1.23M_\odot$, the radius range turns out to be $10.21\,{\rm km} \leqslant R \leqslant 12.21$ km. See Table 1.

The mass of 4U 1608-52 was already estimated to be $M = 1.74 \pm 0.14M_\odot$ (Güver et al. 2010). Thus, the mass parameter has been varied in this range yielding three sets of parameters. The observed QPO frequencies are best reproduced

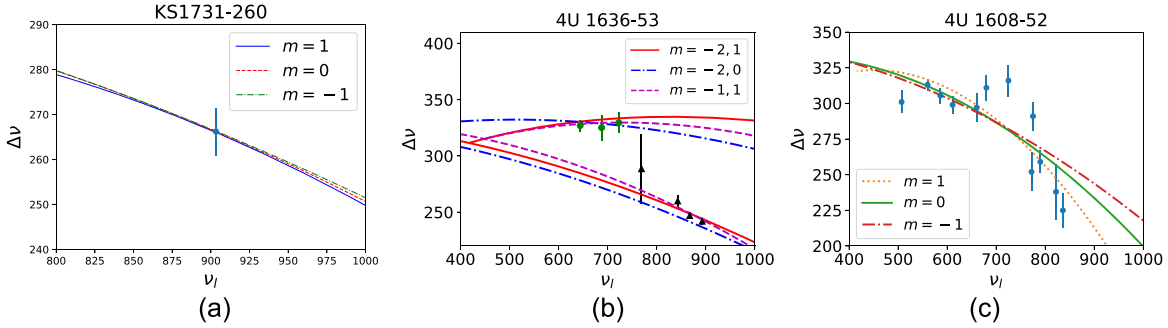

Figure 2. Variation of QPO frequency difference with lower QPO frequency for fast rotators: (a) KS 1731-260, (b) 4U 1636-53, and (c) 4U 1608-52. The points with the error bar are observed data, and the lines correspond to the model fitting. For (b) the data have been fitted for two modes shown by green circles and black triangles. See Table 1 for other details for each source including χ^2.

Table 1
Physical Parameters for Neutron Stars

Fast Rotator	ν_s (Hz)	M ($M_\odot$)	R (km)	m	$\lvert 1-\chi^2\rvert$
KS 1731-260	524	1.51	10.08–12.04	1	−NA-
KS 1731-260	524	1.2	10.32–12.33	0	−NA-
KS 1731-260	524	1.07	10.99–13.14	−1	−NA-
KS 1731-260	524	1.07	8.31–9.93	0	−NA-
4U 1636-53	581.75	1.5	14.52–17.35	−2	0.689
4U 1636-53	581.75	1.65	15.61–18.66	−2	0.797
4U 1636-53	581.75	1.23	10.21–12.21	−1	0.966
4U 1608-52	619	1.87	13.69–16.36	1	2.54
4U 1608-52	619	1.86	11.27–13.47	0	2.47
4U 1608-52	619	1.6	13.08–15.64	−1	2.67
Slow Rotator	ν_s (Hz)	M ($M_\odot$)	R (km)	m	
4U 1702-429	330	1.67	9.25–11.06	1	∼0.00
4U 1702-429	330	0.85	7.62–9.11	0	∼0.00
4U 1702-429	330	1.2	11.98–14.32	−2	∼0.00
4U 1702-429	330	0.97	10.77–12.87	−3	∼0.00
4U 1728-34	364.23	1.99	15.2–18.16	−2	3.046
4U 1728-34	364.23	1.26	11.58–13.84	−3	3.137
4U 1728-34	364.23	0.85	8.88–10.62	−4	3.226
	Estimated ν_s (Hz)				
Sco X-1	300	1.4	22.5–26.9	1	0.35
Sco X-1	600	1.4	15.91–19.08	1	0.35
Sco X-1	662	1.44	10.21–12.2	−1	0.75
Sco X-1	602	1.89	11.71–14	1	0.35

for mass $M = 1.87M_\odot$, with the radius of neutron star in range 13.69–16.36 km; $M = 1.86M_\odot$ with a radius in range 11.27–13.47 km; and finally mass $M = 1.6M_\odot$ with a radius in range 13.08–15.64 km.

5.2. Slow Rotators

The slow rotating neutron stars with known spin frequencies are: 4U 1702-429 (Markwardt et al. 1999) and 4U 1728-34 (van Straaten et al. 2002; Méndez & van der Klis 1999). It is evident from the data that the sources are in the linear regime. By varying the mass and the spin parameter, we obtain the best-fitting parameters. For 4U 1702-429, we find that mass $M = 1.67M_\odot$ gives a radius within 9.25–11.06 km. The other solutions that also fit well with the data correspond to mass $M < 1.4M_\odot$, with the mass being $M = 0.85M_\odot$, $1.2M_\odot$, and $0.97M_\odot$. The corresponding m and radius are given in Table 1 for both of the stars, and the fitting is shown in Figure 3.

However, the relationship between the lower kilohertz QPO frequency (ν_l) and the difference of frequencies ($\Delta\nu$) for 4U 1728-34 does not follow the expected trend where $\Delta\nu$ seems to have a bimodal trend with ν_l. This causes a rather poor fitting of the data by our model for a fixed m, as shown in Figure 3. As discussed in Section 5.1 for the case of 4U 1636-53, it is possible that two harmonics or modes, m_1 and m_2, are activated at different times during observations, and not considering both the modes adequately in the analysis results in a poor fit. Hence, similar to the case of 4U 1636-53, we vary the mass M and spin parameter a for two values of m. This gives two curves simultaneously for a given M and a, which are fitted with the observed data as shown in Figure 4. For this, the estimated mass comes out to be $M = 1.99M_\odot$ with the radius in the range 15.2–18.16 km; $M = 1.26M_\odot$ with the radius in the range 11.58–13.84 km; and $M = 0.85M_\odot$ with the radius in the range 8.88–10.62 km, as mentioned in Table 1. But following Mukhopadhyay (2009), we can stick to mass $M < 1.4M_\odot$.

5.3. Estimate of Spin Frequency for Sco X-1

Sco X-1 is an X-ray binary system with a low-mass companion star of mass approximately $0.42M_\odot$ and a neutron star of mass around $1.4M_\odot$, as reported by Steeghs & Casares (2002) and Messenger et al. (2015). Although the spin frequency of Sco X-1 remains unknown, this source has been observed to exhibit a pair of kilohertz QPO frequencies with $\Delta\nu$ in a range of ∼225–310 Hz (Méndez & van der Klis 2000). Here we vary the mass from $1.35M_\odot$ to $1.45M_\odot$ so that it remains close to $1.4M_\odot$, and we vary the spin frequency ν_s in the range of 200–800 Hz. Now if we consider the nonlinear mode-locking, then the best-fit ν_s turns out to be at 600 Hz for the radius range 15.91–19.08 km, and 662 Hz for the radius range 10.21–12.2 km. However, the former seems to suggest a very high radius and, hence, is uncertain. In the linear regime, i.e., considering it to be a slow rotator, we find that the spin frequency of $\nu_s = 300$ Hz gives an excellent fit with the observed data, as shown in Figure 3. However, it seems to be ruled out due to quite a large possible radius given in Table 1. Although we have varied the mass in a range around $1.4M_\odot$, we still have obtained the best fit to be at $M = 1.4$–$1.44M_\odot$ with all of the corresponding parameters as mentioned in Table 1. If the mass is relaxed to a higher value, e.g., $M = 1.89M_\odot$, then

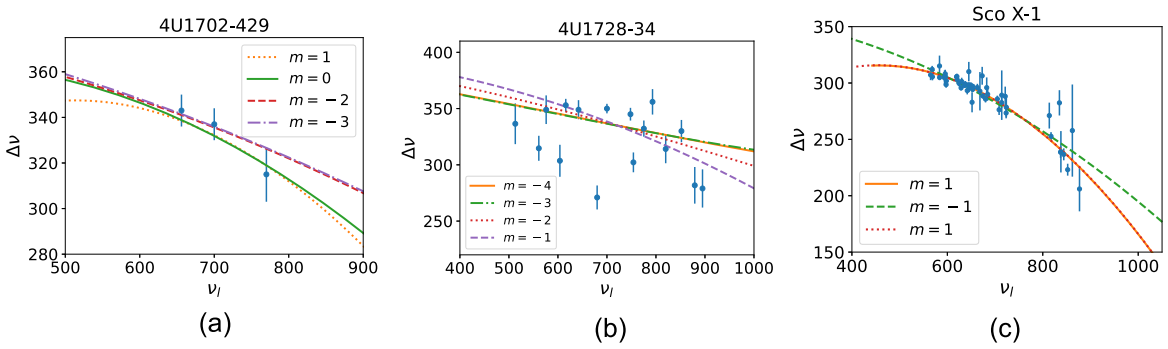

Figure 3. Same as Figure 2, except for two slow rotators: (a) 4U 1702-429, and (b) 4U 1728-34; and (c) Sco X-1 whose spin frequency is not confirmed yet. See Table 1 for other details for each source including χ^2.

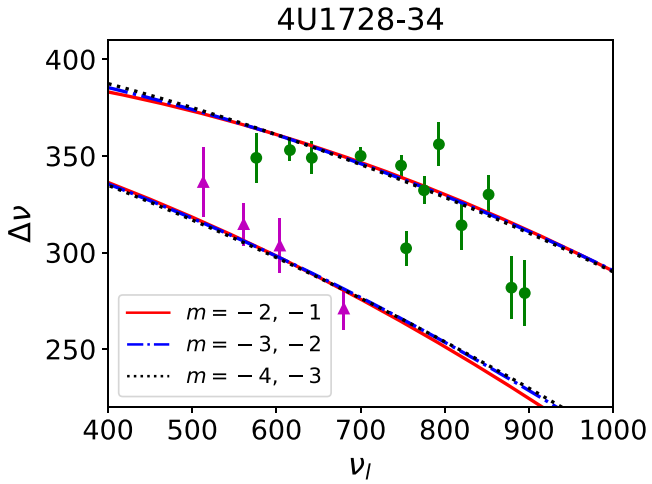

Figure 4. Same as Figure 2, except for 4U 1728-34. The observed QPO frequencies have been fitted for two modes shown by green circle and magenta triangle for a fixed mass and spin parameter. See Table 1 for other details including χ^2.

the best-fit radius range in the nonlinear regime turns out to be 11.71–14 km with $\nu_s = 602$ Hz.

6. Black Hole QPOs

Several black holes with twin HF QPOs have their masses determined through independent observations, such as GRO J1655-40 (Orosz & Bailyn 1997; Shahbaz et al. 1999), XTE J1550-564 (Orosz et al. 2002), GRS 1915+105 (Greiner et al. 2001; Reid et al. 2014), H1743-322 (Miller et al. 2006), and IGR J17091-3624 (Altamirano & Belloni 2012). However, the spin parameter of these black holes remains uncertain. To estimate the spin of these black holes, we fit the observed QPOs to our model and determine the spin parameter that provides the best fit, as summarized in Table 2. We search for the optimal value of a by varying the mass of the black hole within its error bar.

The black hole mass of GRO J1655-40 is still a matter of debate, with some groups estimating it to be $M = 7.02 \pm 0.22 M_\odot$ (Orosz & Bailyn 1997), while others suggest $M = 5.4 \pm 0.3$ (Beer & Podsiadlowski 2002) and $5.31 \pm 0.07 M_\odot$ (Motta et al. 2013). To account for this uncertainty, we consider all of the suggested mass ranges (mass values with the error bars) and estimate the spin parameter. The two HF QPOs now known in this source occur at frequencies of 300 Hz and 450 Hz (Motta et al. 2013). We find that not the entire mass ranges are able to reproduce the observed QPOs. We find that for M to be in $6.82–7.24 M_\odot$ and $5.1–5.48 M_\odot$, the observed QPOs are reproduced when the spin parameter a lies in 0.93–0.89 for $m = -1$ and 0.86–0.61 for $m = -2$, respectively.

Table 2
Physical Parameters for Black Holes

Black Hole	M ($M_\odot$)	Estimated a	ν_h (Hz)	ν_l (Hz)	m
GRO J1655-40	$7.02^{+0.22}_{-0.2}$	0.91 ∓ 0.02	**450**	**300**	−1
GRO J1655-40	$5.4^{+0.08}_{-0.3}$	$0.8^{-0.19}_{+0.06}$	**450**	**300**	−2
XTE J1550-564	10.92-11.07	0.57 ± 0.01	**276**	**184**	−1
XTE J1550-564	10.26-11.58	0.99-0.89	**276**	**184**	−1
H1743-322	9.97-10.91	0.61-0.7	**240**	**163**	−2
H1743-322	9.53-9.61	0.6 ± 0.01	**240**	**163**	−2
H1743-322	9.25-10.86	0.87-0.71	**240**	**163**	−2
XTE J1859+226	5.9-9.69	0.57-0.61	**227.5**	**128.6**	−2
IGR J17091-3624	9.9-10.02	0.59 ± 0.01	164	**66**	−2
IGR J17091-3624	11.04-15.46	0.6-0.67	164	**66**	−2
IGR J17091-3624	8.89-10.63	0.66-0.99	164	**66**	−3
GRS 1915 + 105	$12.4^{+2.0}_{-0.75}$	$0.94^{-0.14}_{+0.05}$	**168**	113	-2
			69	**41**	−6
XTE J1752-223	$10^{+1.63}_{-1.45}$	$0.62^{+0.3}_{-0.2}$	442.91	114.87	−1
GX 339-4	5.3-6.17	0.65-0.99	278.67	127.7	−3
			208.44	105.35	−4
GX 339-4	6.13-6.17	>0.97	278.67	127.7	−3
			208.44	105.35	−4

Note. The boldfaced frequencies are those without dispute as of now.

The mass of the black hole XTE J1550-564 has been taken to be $M = 9.68–11.58 M_\odot$ (Orosz et al. 2002), which shows HF QPOs at frequencies 276 Hz and 184 Hz (Remillard et al. 2002). We find that for the mass M to be in the range of $10.92 M_\odot$ to $11.07 M_\odot$ and $m = -1$, the spin parameter is to be $a = 0.57 \pm 0.01$ in order to obtain observed QPOs by our model. Also, for M to be in $10.26–11.58 M_\odot$, a is estimated to be in 0.99–0.89 for $m = -1$. However, $a = 0.57$ is in very close in agreement with the spin parameter obtained by Fe line fitting as by Steiner et al. (2011b). This leads to a better constraint on the mass of the black hole in XTE J1550-564.

The source H1743-322 has been observed with HF QPO peaks at 240 Hz and 163 Hz (Homan et al. 2005). The mass of this black hole is estimated to be in the range of $9.25–12.86 M_\odot$ (Molla et al. 2017). It has been shown by Steiner et al. (2011a)

that the spin parameter a of this black hole lies in the range of -0.3 to 0.7 and the extreme cases of $a \sim 0.9$ can be ruled out with high confidence. Considering this and after fitting our model best with the observed QPOs, we obtain the mass of the black hole to be in the range of 9.53–9.61$M_\odot$ for $a = 0.6 \pm 0.01$, and in 9.97–10.91$M_\odot$ for $a = 0.61$–0.7, and in range of 9.25–10.86 $M_\odot$ for $a = 0.87$–0.71.

Based on the optical observations in 2017, the black hole XTE J1859+226 during quiescence is estimated to have a mass of $M = 7.8 \pm 1.9 M_\odot$ (Yanes-Rizo et al. 2022). In addition, a pair of QPOs with frequencies of 128.6 and 227.5 Hz was observed in the 1999–2000 outburst of the same black hole transient from RXTE/PCA data (Motta et al. 2022). We hence vary the mass in the above range and find that for the lowest $|m|$ ($m = -2$), leading to the best fit, the spin parameter a comes out to be in 0.57–0.61 for the mass M in the range of 5.9–9.69$M_\odot$.

The estimated mass range for IGR J17091-3624 is 8.7–15.6$M_\odot$ (Iyer et al. 2015) based on spectrotemporal analysis during the onset of the 2011 outburst. However, Altamirano & Belloni (2012) argued that the QPO peak at 164 Hz is a marginal detection, while that at 66 Hz is reliable. In our study, we vary the mass within the above-mentioned range, and reproduce both the QPO frequencies. We however find that the entire mass range does not reproduce these QPOs. We have tabulated in Table 2 the result for $m = -3$, which shows that the source could have a fast spinning black hole. The results with $m = -2$, however, argue for the spin parameter of $a \sim 0.59$–0.67. Thus, our results give new constraints on the mass.

The twin HF QPOs of GRS 1915 + 105 had been reported to be at 67 and 40 Hz (Strohmayer 2001), while 67 Hz alone was reported even earlier (Morgan et al. 1997). An additional twin peak of ∼168 Hz and ∼113 Hz were reported further (McClintock & Remillard 2006; Belloni et al. 2006). However, later on, a prominent QPO around 70 Hz was observed by various groups; see Belloni et al. (2019) and Majumder et al. (2022) for the observation of AstroSat. Moreover, a very sporadic appearance of peaks at 41 Hz and 34 Hz was also reported (Belloni et al. 2006; Belloni & Altamirano 2013). The mass of the source has been estimated to lie in the range of 10.6–14.4$M_\odot$ (Reid et al. 2014) by independent observation. However, only the mass range 11.65–14.4$M_\odot$ with varying spin parameter a in the range of 0.99–0.8, for $m = -2$, is successful in reproducing the QPOs at 168 Hz and 113 Hz. For the very similar mass and spin combinations, the pair of 69 Hz and 41.1 Hz is reproduced by our model but for $m = -6$. However, note that 40 Hz QPOs are observed in the harder state (Strohmayer 2001) with the X-ray energy band above 13 KeV, while the current model mostly is in accordance with the Keplerian accretion disk corresponding to the high/soft state (see, however, Section 7). For the mass of 12.4$M_\odot$ the spin parameter is estimated to be $a = 0.94$. Thus, notice from this analysis that we are further able to constraint the lower bound of the black hole mass, due to a theoretical upper limit of the spin parameter. A more precise measurement of the mass will lead to a more accurate estimate of the spin parameter.

The mass of XTE J1752-223 has been estimated to be in the range of 3.1–55$M_\odot$ (Nakahira et al. 2012). However, Belloni et al. (2012) suggested that the observed HF QPO frequencies, 442.91 Hz and 114.97 Hz, are likely to be statistical fluctuations, neither in the 3:2 ratio. Some observations reported its spin to be in the intermediate range with $a \sim 0.52 \pm 0.11$ (Reis et al. 2011). However, a very recent analysis showed that the mass of XTE J1752-223 can be constrained in the range $10 \pm 1.9 M_\odot$ (Debnath et al. 2021). Nevertheless, if the above-mentioned QPO frequencies turned out to be real, we find a better constraint on the mass of $10^{+1.63}_{-1.45} M_\odot$ and the spin parameter, to be in the range of $a \sim 0.6$–0.65, for $m = -1$ for the best fit of QPOs by our model.

While reporting four HF QPO frequencies of GX 339-4, 105.35 Hz, 127.7 Hz, 208.44 Hz, and 278.64 Hz, Belloni et al. (2012) argued that all of them are spurious/nonreal. The mass of the black hole GX 339-4 has been varied in the range of $M = 5.8 \pm 0.5 M_\odot$ (Hynes et al. 2003). If we indeed relied upon the questionable QPO frequencies mentioned above, assuming them to form two pairs as 127.7, 278.64 Hz and 105.35 Hz, 208.44 Hz (Belloni et al. 2012), we can further constraint the mass of the source. Interestingly, varying the mass within the given range does not provide suitable parameters that could reproduce both frequency pairs assuming a fixed mode (m). However considering each pair corresponds to a distinct mode, i.e., mode m changes for different pairs, both the pairs of QPO frequencies are reproduced. We find that the mass in the range of 5.3–6.17$M_\odot$ with the spin parameter of $a = 0.99$–0.65 is able to reproduce first and second frequency pairs for $m = -3$ and -4, respectively. While Ludlam et al. (2015) argued for a spin parameter $a > 0.97$, our analysis suggests that such a value can only be obtained for $M = 6.15$–6.17$M_\odot$, which provides a better constraint on the mass of the black hole GX 339-4.

7. Explaining other QPOs

The HF/kilohertz QPOs need not necessarily always appear in a pair, as is evident observationally (see, e.g., Homan et al. 2003; Belloni et al. 2012; Remillard & Morgan 1999). We argue that when the peak separation $\Delta\nu = 0$, i.e., when both of them coincide with equal amplitude, they exhibit only one QPO. From Equation (35) for $b_1 = -b_2$, we can write

$$\nu_1 - \nu_2 = \frac{n - m + 1}{b_1} \nu_s. \tag{46}$$

Further, we modify the proposal given by Equation (37) for general b_1 as

$$\nu_h = \nu_1 + \frac{m + 1}{b_1} \nu_s, \quad \nu_l = \nu_2 + \frac{m}{b_1} \nu_s. \tag{47}$$

Therefore, from Equations (46) and (47), we obtain

$$\nu_h - \nu_l = \Delta\nu = \frac{n - m + 2}{b_1} \nu_s. \tag{48}$$

Hence, $\Delta\nu = 0$, either for higher-order nonlinearity, which corresponds to a very large b_1 or for $n = m - 2$. For the latter, the mode-locking has to be led by $\nu_h - \nu_l = 0$, rather than $\nu_1 - \nu_2 = 0$.

For the low-frequency QPOs, as seen in the hard states of GRS 1915+105 (Belloni et al. 2006), we must consider nonzero u_r and its radial gradient γ. This is because a hard accretion state implies significant radial velocity, making the flow hot and radiation trapped (see, e.g., Narayan & Yi 1995; Chakrabarti 1996; Rajesh & Mukhopadhyay 2010). Therefore, any model should include u_r. Therefore, minimizing $f(\omega)$ in

Equation (29) with $\gamma \neq 0$, we obtain

$$\omega^2 = X - \frac{\gamma^2}{2} \pm \frac{\sqrt{\gamma^4 - 4X\gamma^2}}{2}, \quad (49)$$

where $X = \Omega_\phi(\xi + 2\Omega_\phi) + \Omega_r^2$. Now in an advective sub-Keplerian flow $\Omega_\phi \sim r^{-q}$, where $q > 1.5$, and $\gamma^2 >> \Omega_r^2$. Therefore, from Equation (49) we obtain the physically meaningful resonance frequency leading to maximum amplitude of radial and azimuthal perturbations as

$$\omega = \frac{\sqrt{2}\,\Omega_r^2}{\gamma}, \quad (50)$$

for $q = 2$. For an advective accretion disk with α-viscosity $= 0.01$ around a rotating black hole of spin (Kerr) parameter $a = 0.99$ (Rajesh & Mukhopadhyay 2010), the low-frequency QPO turns out to be $\gtrsim$0.1 Hz based on the above model. Such a QPO frequency is observed in the hard state of GRS 1915+105.

A detailed analysis of the above-mentioned QPOs based on our model will be presented elsewhere. The present section just imprints that the same model is capable of explaining all kinds of QPOs.

8. Summary and Conclusions

The origin of QPOs is a longstanding problem, particularly in high-energy astrophysics. Over the years, several models have been proposed to enlighten the issue. However, none of them is without any caveat. Moreover, there are several classes of QPOs observed, ranging from millihertz to kilohertz orders, for the black hole, neutron star, and white dwarf sources. The question is then, are the origins of all QPOs the same? The HF QPOs, e.g., around black holes, are mostly observed in softer states, while the ones of the order of hertz or tenths of hertz are observed in harder states. The present work aims to provide a unified QPO model. We show that HF and kilohertz QPOs from black holes and neutron stars, respectively, are of the same origin. Other QPOs are also expected to originate from the same basic mechanism, established in the work.

We have shown explicitly that QPOs of frequency ~100–1000 Hz originate from the same mechanism. We have shown that fundamental epicyclic oscillation frequency is modified in the accretion disk compared to what it is for a test particle. When the disk is perturbed by external forces including that due to frame-dragging effects by the spinning compact object at the center, the new modes with frequencies in the combination of fundamental and perturbation frequencies are formed, and they form a resonance around a particular radius. This resonance leads to the locking of new modes, which correspond to higher and lower QPO frequencies.

Now the question is, whether the other QPOs, including those with low frequency, originate from the same mechanism or not. This is particularly important, as some other models, e.g., that of Chakrabarti & Manickam (2000), are apparently capable of explaining observed low-frequency QPOs in black hole systems. Similarly, the QPOs also appear without their twin. Can the present model be applicable to a single HF/kilohertz QPO? It is possible to have the latter when $\Delta\nu \sim 0$, i.e., practically one peak is (or both peaks overlap each other), and for higher-order nonlinearity or resonance mode-locking at $\nu_h - \nu_l = 0$, in place of $\nu_1 - \nu_2 = 0$. The former, however, corresponds to nonzero radial velocity and its gradient. Indeed the low-frequency QPOs appear in the hard state of X-ray binaries when the accretion flow is understood to have a significant advection and be radiation trapped hot. The new resonance condition with the maximum amplitude of the perturbation with a nonzero radial velocity gradient could explain low-frequency QPOs. The details will be reported elsewhere. Therefore, in principle, the present model appears to be a truly unified model.

Our model also predicts and/or constraints the mass of the black holes and neutron stars, particularly if not known for the latter from an independent estimate. It also predicts the radius of neutron stars.

It is also possible that Einstein's theory of general relativity (GR) may not be the ultimate theory of gravity, and there may be some modifications to GR (e.g., Das & Mukhopadhyay 2015; Kalita & Mukhopadhyay 2018, 2019; Das & Mukhopadhyay 2022) that could explain the observed varieties of QPOs more judiciously based on the present QPO model. Since QPO is expected to emerge from close to the black hole, such modification to GR can be captured by the QPO frequencies.

Acknowledgments

The authors thank Tomaso Belloni for bringing to our attention the latest data, carefully reading the manuscript, comments, and suggestions. The authors also thank the referee for providing comments that have helped to improve the clarity of this paper, including that in the presentation of results in the tables. A.R.D. acknowledges the financial support from KVPY, DST, India. B.M. thanks SERB, India, with Ref. No. CRG/2022/003460, for partial support toward this research.

ORCID iDs

Arghya Ranjan Das https://orcid.org/0000-0001-8451-0806
Banibrata Mukhopadhyay https://orcid.org/0000-0002-3020-9513

References

Abramowicz, M. A., Bulik, T., Bursa, M., & Kluźniak, W. 2003a, A&A, 404, L21
Abramowicz, M. A., Karas, V., Kluzniak, W., Lee, W. H., & Rebusco, P. 2003b, PASJ, 55, 466
Altamirano, D., & Belloni, T. 2012, ApJL, 747, L4
Beer, M. E., & Podsiadlowski, P. 2002, MNRAS, 331, 351
Bejger, M., & Haensel, P. 2002, A&A, 396, 917
Belloni, T., Méndez, M., & Homan, J. 2005, A&A, 437, 209
Belloni, T., Méndez, M., & Homan, J. 2007, MNRAS, 376, 1133
Belloni, T., Soleri, P., Casella, P., Méndez, M., & Migliari, S. 2006, MNRAS, 369, 305
Belloni, T. M., & Altamirano, D. 2013, MNRAS, 432, 19
Belloni, T. M., Bhattacharya, D., Caccese, P., et al. 2019, MNRAS, 489, 1037
Belloni, T. M., Sanna, A., & Méndez, M. 2012, MNRAS, 426, 1701
Blaes, O. M., Šrámková, E., Abramowicz, M. A., Kluźniak, W., & Torkelsson, U. 2007, ApJ, 665, 642
Blandford, R. D., & Znajek, R. L. 1977, MNRAS, 179, 433
Cadez, A., Calvani, M., & Kostic, U. 2008, A&A, 487, 527
Chakrabarti, S. K. 1996, ApJ, 464, 664
Chakrabarti, S. K., & Manickam, S. G. 2000, ApJL, 531, L41
Connors, P. A., Piran, T., & Stark, R. F. 1980, ApJ, 235, 224
Cook, G. B., Shapiro, S. L., & Teukolsky, S. A. 1994, ApJ, 424, 823
Das, A. R., & Mukhopadhyay, B. 2022, EPJC, 82, 939
Das, U., & Mukhopadhyay, B. 2015, JCAP, 2015, 045
Davis, S. W., Blaes, O. M., Hubeny, I., & Turner, N. J. 2005, ApJ, 621, 372
Debnath, D., Chatterjee, K., Chatterjee, D., Jana, A., & Chakrabarti, S. K. 2021, MNRAS, 504, 4242
Dovčiak, M., Karas, V., & Yaqoob, T. 2004, ApJS, 153, 205

Franchini, A., Motta, S. E., & Lodato, G. 2016, MNRAS, 467, 145
Germana, C., Kostic, U., Cadez, A., & Calvani, M. 2009, in AIP Conf. Proc. 1126, Tidal Disruption of Small Satellites Orbiting Black Holes, ed. J. Rodriguez & P. Ferrando (Paris: AIP), 367
Greiner, J., Cuby, J. G., & McCaughrean, M. J. 2001, Natur, 414, 522
Güver, T., Özel, F., Cabrera-Lavers, A., & Wroblewski, P. 2010, ApJ, 712, 964
Homan, J., Klein-Wolt, M., Rossi, S., et al. 2003, ApJ, 586, 1262
Homan, J., Miller, J. M., Wijnands, R., et al. 2005, ApJ, 623, 383
Hynes, R. I., Steeghs, D., Casares, J., Charles, P. A., & O'Brien, K. 2003, ApJL, 583, L95
Iyer, N., Nandi, A., & Mandal, S. 2015, ApJ, 807, 108
Jonker, P. G., Mé ndez, M., & van der Klis, M. 2002, MNRAS, 336, L1
Kalita, S., & Mukhopadhyay, B. 2018, JCAP, 2018, 007
Kalita, S., & Mukhopadhyay, B. 2019, EPJC, 79, 877
Kluzniak, W., & Abramowicz, M. A. 2002, arXiv:astro-ph/0203314
Kluźniak, W., Abramowicz, M. A., Kato, S., Lee, W. H., & Stergioulas, N. 2004, ApJL, 603, L89
Kostic, U., Cadez, A., Calvani, M., & Gomboc, A. 2009, A&A, 496, 307
Kotrlová, A., Šrámková, E., Török, G., et al. 2020, A&A, 643, A31
Kulkarni, A. K., Penna, R. F., Shcherbakov, R. V., et al. 2011, MNRAS, 414, 1183
Lamb, F. K., & Miller, M. C. 2001, ApJ, 554, 1210
Landau, L. D., & Lifshitz, E. M. 1976, Mechanics (Oxford: Pergamon)
Li, L.-X., Zimmerman, E. R., Narayan, R., & McClintock, J. E. 2005, ApJS, 157, 335
Lightman, A. P., & Shapiro, S. L. 1975, ApJL, 198, L73
Ludlam, R. M., Miller, J. M., & Cackett, E. M. 2015, ApJ, 806, 262
Majumder, S., Sreehari, H., Aftab, N., et al. 2022, MNRAS, 512, 2508
Markwardt, C. B., Strohmayer, T. E., & Swank, J. H. 1999, ApJL, 512, L125
Mauche, C. W. 2002, ApJ, 580, 423
McClintock, J. E., & Remillard, R. A. 2006, in Compact Stellar X-ray Sources, ed. W. Lewin & M. van der Klis (Cambridge Astrophysics: Cambridge Univ. Press), 157
Messenger, C., Bulten, H. J., Crowder, S. G., et al. 2015, PhRvD, 92, 023006
Miller, J. M., Raymond, J., Homan, J., et al. 2006, ApJ, 646, 394
Molla, A. A., Chakrabarti, S. K., Debnath, D., & Mondal, S. 2017, ApJ, 834, 88
Morgan, E. H., Remillard, R. A., & Greiner, J. 1997, ApJ, 482, 993
Motch, C., Ricketts, M., Page, C., Ilovaisky, S., & Chevalier, C. 1983, A&A, 119, 171
Motta, S., Homan, J., Muñoz-Darias, T., et al. 2012, MNRAS, 427, 595
Motta, S. E., Belloni, T., Stella, L., et al. 2022, MNRAS, 517, 1469
Motta, S. E., Belloni, T. M., Stella, L., Muñoz-Darias, T., & Fender, R. 2013, MNRAS, 437, 2554
Mukhopadhyay, B. 2009, ApJ, 694, 387
Mukhopadhyay, B., Ray, S., Dey, J., & Dey, M. 2003, ApJL, 584, L83
Méndez, M., & van der Klis, M. 1999, ApJL, 517, L51
Méndez, M., & van der Klis, M. 2000, MNRAS, 318, 938
Méndez, M., van der Klis, M., Wijnands, R., et al. 1998, ApJL, 505, L23
Nakahira, S., Koyama, S., Ueda, Y., et al. 2012, PASJ, 64, 13
Narayan, R., & Yi, I. 1995, ApJ, 452, 710
Nayfeh, A., & Mook, D. 1979, Nonlinear Oscillations (New York: Wiley)
Nowak, M. A., Wagoner, R. V., Begelman, M. C., & Lehr, D. E. 1997, ApJL, 477, L91
Orosz, J. A., & Bailyn, C. D. 1997, ApJ, 477, 876
Orosz, J. A., Groot, P. J., van der Klis, M., et al. 2002, ApJ, 568, 845
Özel, F., Gould, A., & Güver, T. 2012, ApJ, 748, 5
Pétri, J. 2005, A&A, 439, 443
Rajesh, S. R., & Mukhopadhyay, B. 2010, MNRAS, 402, 961
Rebusco, P. 2004, PASJ, 56, 553
Rebusco, P. 2008, NewAR, 51, 855
Reid, M. J., McClintock, J. E., Steiner, J. F., et al. 2014, ApJ, 796, 2
Reis, R. C., Miller, J. M., Fabian, A. C., et al. 2011, MNRAS, 410, 2497
Remillard, R. A., & McClintock, J. E. 2006, ARA&A, 44, 49
Remillard, R. A., & Morgan, E. H. 1999, AAS Meeting, 195, 37.02
Remillard, R. A., Muno, M. P., McClintock, J. E., & Orosz, J. A. 2002, ApJ, 580, 1030
Reynolds, C. S., & Fabian, A. C. 2008, ApJ, 675, 1048
Reynolds, C. S., & Nowak, M. A. 2003, PhR, 377, 389
Rezzolla, L., Yoshida, S., Maccarone, T. J., & Zanotti, O. 2003, MNRAS, 344, L37
Shahbaz, T., van der Hooft, F., Casares, J., Charles, P. A., & van Paradijs, J. 1999, MNRAS, 306, 89
Smith, D. A., Morgan, E. H., & Bradt, H. 1997, ApJL, 479, L137
Steeghs, D., & Casares, J. 2002, ApJ, 568, 273
Steiner, J. F., McClintock, J. E., & Reid, M. J. 2011a, ApJL, 745, L7
Steiner, J. F., Reis, R. C., McClintock, J. E., et al. 2011b, MNRAS, 416, 941
Stella, L., & Vietri, M. 1998, ApJL, 492, L59
Stella, L., Vietri, M., & Morsink, S. 1999, ApJL, 524, L63
Strohmayer, T. E. 2001, ApJL, 552, L49
Titarchuk, L., & Wood, K. 2002, ApJL, 577, L23
Torok, G., Bakala, P., Sramkova, E., Stuchlik, Z., & Urbanec, M. 2010, ApJ, 714, 748
Torok, G., Kotrlova, A., Sramkova, E., & Stuchlik, Z. 2011, A&A, 531, A59
Török, G., Goluchová, K., Horák, J., et al. 2015, MNRAS, 457, L19
van der Klis, M. 2000, ARA&A, 38, 717
van der Klis, M., Jansen, F., van Paradijs, J., et al. 1985, Natur, 316, 225
van Straaten, S., van der Klis, M., di Salvo, T., & Belloni, T. 2002, ApJ, 568, 912
Woudt, P. A., & Warner, B. 2002, MNRAS, 333, 411
Yanes-Rizo, I. V., Torres, M. A. P., Casares, J., et al. 2022, MNRAS, 517, 1476
Zhang, S. N., Cui, W., & Chen, W. 1997, ApJL, 482, L155